PROJECT COMPLETION REPORT

Title of the project: **Fluorescent nanocrystal-induced ion channels for biomolecular labeling applications**

File number: **100/IFD/3932/2009-10** dated **25.08.2009 dispatched on 31.08.2009**

Names and addresses of the investigation:

Dr. Dambarudhar Mohanta
Principal Investigator
Department of Physics
Tezpur University
Napaam-784028
Assam

1. Title of the project: **Fluorescent nanocrystal-induced ion channels for biomolecular labeling applications**

2. Principal Investigator(s) and Co-Investigator(s): **Dr. Dambarudhar Mohanta**

3. Implementing Institution(s) and other collaborating Institution(s): **Tezpur University**

4. Date of commencement: Sanctioned on **25.08.2009** ;
    Dispatched on **31.08.2009;**
    Joining of the JRF on **17.11.2009;**

5. Planned date of completion: **16.11.2012**

6. Actual date of completion: **16.11.2012**

7. Objectives as stated in the project proposal:
    - Synthesis and stabilization of fluorescent nanocrystals.
    - Conjugation of nanocrystal with ion channel proteins.
    - Ion channel response of unconjugate NCs and bio-conjugate NCs, simultaneous electrical and optical Recording to establish the correlation between signaling and fluorescent probes, investigation of magnetic field on ion channels and mechanism of resonance energy transfer in nano-bioconjugates.

    Work plan (including detailed methodology and time schedule): as mentioned in the project proposal.

    Year 1: (a) Installation of Faraday-cage and electrophysiology set up.
    (b) Arrangements for obtaining stable bilayer, preliminary study of ion channels with synthesized quantum dots (QDs).

    Year 2: (a) Experiments with quality fluorescent nanoparticles and evaluation of voltage gated ion channels. Simultaneous measurement of optical and electrical recording.

    Year 3: (a) Analysis of results on ion channels and introduction of a theoretical model, Consideration of the use of a static and alternating magnetic field.

8. Deviation made from original objectives if any, while implementing the project and reasons thereof:

    Fluorescent quantum dots of (CdSe, MnSe etc.) have been fabricated in a control environment. The evidence of QD-induced ion channels has been realized to a great extent and the nature of channel was explored with relevant theoretical treatments. To be honest, the application of magnetic field and simultaneous optical and electrical recording could not be achieved in this project due to lack of additional infrastructure which involved both cost and time. In future, we will be looking into those aspects. Also note that, due to the late receipt of the financial assistance the theoretical modeling was carried out first, while experiments were performed only after the installation of the electrophysiology setup.

9. Experimental work giving full details of experimental set up, methods adopted, data collected supported by necessary table, charts, diagrams & photographs: The year-wise break-ups are as detailed below.

Year 1: (1) Extensive literature survey

Prior to experimental investigation, it was extremely important to understand the structural, physical, mechanical properties of biomembranes, planar lipid bilayers, micelles, vesicles, and proteins. Ion channels represent ion conducting pathways which generally depend on the nature of their gating. In the past, apart from the nature of pore formation, there has been a great deal of interest with regard to channel forming peptides including alamethicin, magainin, gramicidin etc. [1-3]. The amino acid composition, amphipathicity, cationic charge, conformation and structure, hydrophobicity, and size are the characteristics which affect the antimicrobial activity with high specificity, thereby allowing them to attach and insert into the membrane bilayers, and resulting in the formation of ion conducting pathways/pores [4]. The pore formation can be explained by 'barrel-stave'[5], 'carpet'[6] or 'toroidal-pore'[7] mechanisms. In recent decades, alamethicin ion channel proteins have been extensively studied to reveal discrete conductance levels and the nature of channels was discussed in the light of barrel stave mechanism [8-10]. Practically, both patch-clamp and planar lipid bilayer experiments allow studies with regard to the function of single ion channels [11]. In the recent years, solid supported bilayer experiments were shown to be better options over patch-clamp ones owing to several advantages, including viable cost, preparatory conditions, simplicity of designing, reliable and fast data acquisition [12]. In this context, a critical literature survey was performed with regard to technical details of planer chip technology based bilayer experiments which includes bilayer formation [13], bilayer thinning, aperture creation etc [14]. Information with regard to acquisition of data, sources of noise and influence on recording signal, signal bandwidth etc. was also gathered. In planar chip technique, the ion channel response, to a great extent, is influenced by the thermal and electromagnetic noise and the effective bilayer capacitance arising due to the specific characteristic properties of the substrate materials. Also, it may be noted that, substrates having good mechanical and thermal stability are believed to support a very stable bilayer.

(2) Optimization of suitable environment for electrophysiology experiments

The effective bilayer capacitance in a lipid bilayer experiment is given by [15]
$$C_t = C_m + C_s + C_{el}, \tag{1}$$
where C_m = Membrane capacitance, C_{el} = Capacitance of the immersed electrodes, and C_s = Capacitance of the substrate material where,
$$C_s = \varepsilon_r \varepsilon_0 \frac{A}{d} \tag{2}$$
A is the area of the substrate material, ε_r is the dielectric constant of the substrate material, ε_0 is the permittivity in free space; and d is the thickness of the substrate material.

As the nature of ion channels is largely influenced by the background noise, therefore, determination of the individual sources of noise as well as minimization of these are very much essential. Note that, for conventional ion channel experiments, a bilayer has to be supported on the micropore of a substrate material. The nature of thermal energy dissipation results in thermal noise from this dielectric material and this type of noise is known as dielectric noise. The power spectral density and the r.m.s dielectric noise are given by equations (3) and (4) respectively [16]
$$S_D^2(f) = 8\pi k T D C_s f \tag{3}$$

$$I_D = \sqrt{4KTDC_s \pi c_2 f_c^2}, \tag{4}$$

where D is the dissipation factor of the material(s), C_s is the capacitance of the dielectric(s), f_c is the cut-off frequency, $c_2 = 1.3$ for a noise source with a power spectral density that grows linearly as a function of f.

In a quest for obtaining a suitable environment for employing planar chip technology meant for ion channel/electrophysiology experiments, we have made an extensive study on various substrate materials teflon (PTFE), polystyrene (PS), polypropylene (PP), polyethylene terephthalate (PET), poly (methyl methacrylate) (PMMA), quartz, glass, mica and silicon of different dielectric constant, thickness and cross sectional area. For a meaningful analysis, following parameters have been selectively chosen for evaluation.
(i) Variation of capacitance with (a) dielectric constant, (b) area in the range of 0.5- 4.0 cm^2 (at constant substrate thickness within 150 -300 μm), (c) substrate thickness in the range of 100 to 500 μm (for an area of ~1.76 cm^2)
(ii) The variation of r.m.s dielectric noise with dissipation factor and thickness of different materials (with C_{se}=10pF, and f_c=10 kHz). Some of our results are as given below.

We have observed that, for an area of the order of ~1.75 cm^2 of (borosilicate glass), it gives low capacitance in the range 25-45 pF (Fig. 1). Furthermore, polymers such as PTFE, PP, PS, PET, PMMA and quartz exhibit low values of capacitance (~10-40 pF) as for the effective area of 1.75cm^2, and substrate thickness of 150-300 μm (not shown). The borosilicate glass (D=0.0007, f= 10 kHz), contributes only weakly to the r.m.s dielectric noise (~0.25 pA) (Fig. 2). Similarly, quartz, mica and polymers (PTFE, PS) are characterized by very low dielectric noise values. However, as bilayer stability depends largely on the mechanical and thermal resistance of the substrate material, polymer materials are considered as poor supports to hold a bilayer. On the other hand, stability of the bilayer can be retained by use of materials such as, borosilicate glass (Y=45 GPa, m_p=820°C), quartz (Y=71.7 GPa, m_p=1650°C) etc.
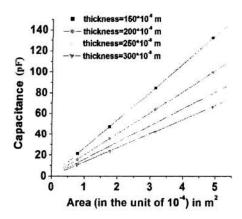

Fig. 1: Characteristic change of capacitance with the area of the electrolytic chamber made on definite substrate glass.
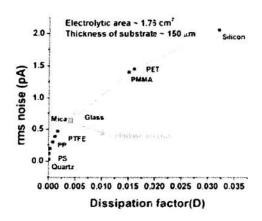
Fig. 2: Variation of r.m.s dielectric noise with dissipation factor for a number of substrate materials

Year 2: (1) Dynamics of QDs in non-aggregated and aggregated (ion channel forming) states in the theoretical framework

The use of semiconductor nanocrystals, in biological application, has emerged as an important aspect in the major biophysical areas of research due to their novel optical properties [17-19]. As many of the applications of QDs in cell biology involve interaction with lipid bilayer membranes, the behavior of QDs on these structures is of significant interest to the world-wide scientific communities.

The mean square displacement, MSD ($<r^2>$) of a QD (having diameter d) undergoing Brownian motion in a free solution with viscosity of the solvent (η_s) is given by,

$$<r^2>=4D_0t. \tag{5}$$

Here, $D_0=\dfrac{kT}{3\pi\eta_s d}$ [20] is the diffusion coefficient of the QD and t is the diffusion time, k and T are Boltzmann constant and absolute temperature; respectively. The relaxation time (τ) i.e., time in which QDs undergo Brownian motion to a distance equal to the radius of the QD and experience successive collisions in the electrolytic solution can be expressed by:

$$\tau=\frac{\left(\frac{d}{2}\right)^2}{\left(\frac{kT}{3\pi\eta_s d}\right)} . \tag{6}$$

In solution, diffusion is dependent on the QD concentration (C) because of interdot interaction. In this case, the MSD and relaxation time of a QD in an electrolytic solution can be rewritten as:

$$<r^2>=4D_{cl}t \tag{7}$$

$$\tau = \frac{\left(\frac{d}{2}\right)^2}{[D_c(1-\lambda C)]} \tag{8}$$

4

In lipid bilayer, the water soluble QDs are attracted to the bilayer by electrostatic interaction existing between net negative charges of QDs and the cationic head-groups of the lipid bilayer [21]. Across the lipid bilayer, application of an electric field would produce a torque in the QD dipoles, enforcing QDs to insert into the lipid bilayer.

For a spherical QD having radius r, the MSD $(<r^2>)$ in lipid bilayer of thickness h is given by

$$<r^2>=4D_L t \qquad (9)$$

Here, $D_L = \frac{kT}{4\pi\eta_m h}[\ln(\lambda l) - \gamma]$ [19] is the free diffusion coefficient of the QD in lipid bilayer. Here, η_m and η are viscosities of the membrane (1 poise) and membrane surrounding fluid (0.01 poise); respectively $\lambda_l = \frac{\eta_m h}{\eta(\frac{d}{2})}$, and $\gamma = 0.57$ is the Euler's constant [22].

The relaxation time, in this case, is given by

$$\tau = \frac{\left(\frac{d}{2}\right)^2}{\left[\frac{kT}{4\pi\eta_m h}[\ln(\lambda_l)-\gamma]\right]} . \qquad (10)$$

Considering QD concentration of C and dipole-dipole interaction in lipid bilayer, the expression for MSD and relaxation time can be stated as,

$$<r^2>=4\left\{\frac{kT}{4\pi\eta_m h}[\ln(\lambda_l) - \gamma](1+ \lambda C)\right\}t \qquad (11)$$

$$\tau = \frac{\left(\frac{d}{2}\right)^2}{\left[\frac{kT}{4\pi\eta_m h}[\ln(\lambda_l)-\gamma](1+\lambda C)\right]} \qquad (12)$$

As reported earlier, upon insertion into the lipid bilayer, the QDs aggregate and form ion conducting pores (interface region). The diameter of the pore (d_{pore}) formed as a result of aggregation of N number of QDs is given by [23]

$$d_{pore}= d_{dot}\left(\frac{1}{\frac{\sin\pi}{N}} -1\right) \qquad (13)$$

Here, d_{dot} is the diameter of an individual QD participating in the formation of a nanopore. The conductance state (G) and the diameter of QDs forming a pore can be related as [21],

$$G= \frac{\sigma \pi d_{pore}^2}{4 d_{dot}}$$

Therefore,
$$d_{pore} = \left(\frac{4 d_{dot} G}{\sigma \pi}\right)^{\frac{1}{2}} \qquad (14)$$

Here, σ is the conductivity of the bulk solution (98 mS/cm of 1M KCl+20 mM HEPES buffer at pH 7.5) [21] generally used in the lipid bilayer experiment. We can examine the translational Brownian motion (MSD and τ) of the aggregated structure, as for the conductance state G, by substituting d_{dot} (diameter of QD) by d_{pore} (diameter of the QD forming pore) in Eqn.(15) and Eqn.(16); respectively.

The MSD of the aggregated structure, during the current burst, can be expressed as,

$$<r^2>=4\left\{\frac{kT}{4\pi\eta_m h}[\ln(\lambda_l) - \gamma]\right\}t \qquad (15)$$

Consequently, the relaxation time i.e., the time needed for moving a distance equal to the radius of the pore will be

$$\tau = \frac{\left(\frac{d_{pore}}{2}\right)^2}{D_{LA}} \qquad (16)$$

Here, $D_{LA}=\frac{kT}{4\pi\eta_m h}[\ln(\lambda_l) - \gamma]$ is the diffusion coefficient of the conductive QD ion channel in the lipid bilayer.

We have performed a critical analytical study on QD movement in the electrolytic solution as well as in the lipid bilayer environment. In lipid bilayer, both pre-aggregated and aggregated pore forming QDs are considered with special consideration of partial insertion and fully insertion across the bilayer. For this purpose, 2 types of

5

QDs, one is smaller (2 nm) and other one larger (12 nm) than the lipid bilayer thickness (~4 nm) were chosen. In each case, we considered a constant diffusion time ~0.1 sec for the calculation of MSD. Fig. 3 (a-d), depicts behavior of the Brownian response of the QDs in different environment with special consideration to complete insertion and partial insertions. Note that, in the lipid bilayer, QDs satisfy confined diffusion and directed diffusion along with the simple diffusion phenomena [24]. A special emphasis is given to the simple diffusion of QDs, in all the cases, while considering following characteristics.

(i) Variation of mean square displacement (MSD) a   me with (a) QDs size in the range of (~2-20 nm) in electrolytic solution and in lipid bilayer in the pr   ate (b) Concentration of QDs (in the range of ~1-10 μM) of size 2 nm and 20 nm in the electrolytic solution and in the lipid bilayer, in their pre-aggregated state (assuming dipole-dipole interaction).

(ii) Variation of MSD and relaxation time with nos. of aggregated QDs of different sizes (in the range of ~2-20 nm) in the aggregated structure.

(iii) The variation of conductance state, MSD and relaxation time with no. of aggregated QDs, in both partial and fully inserted cases.
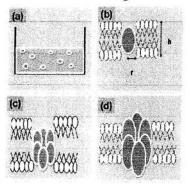
Some of our results are as given below.

Fig. 3: Schematics representing behavior of the QDs in (a) electrolytic solution and (b) in pre-aggregated state in the bilayer. The QD aggregated state with full insertion and partial insertion cases are depicted in (c) and (d).
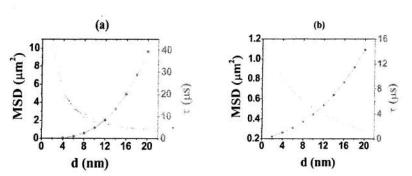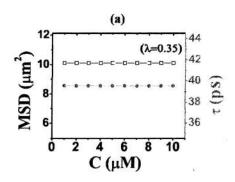

Fig. 4: MSD and τ vs. size of the QDs in (a) electrolytic solution (b) in the lipid bilayer in the pre-aggregated state

It can be observed that, in both electrolytic solution (Fig. 4(a)) and in the pre-aggregated state in the lipid bilayer (Fig. 4(b)), MSD (and relaxation time) rapidly decreases (and increases). Note that, in the lipid bilayer, the MSDs are 10 times smaller than that was found in case of electrolytic media and are consistent with the previous experimental observations [14]. The reduction of MSD is attributed to the comparatively higher viscosity of the bilayer than the electrolytic solution. In contrast, compared to the electrolytic solution, the relaxation time has increased substantially for ~2 nm QDs signifying that smaller sized QDs become more localized across the lipid bilayer.

Taking into account interdot separation as ~2 nm in the electrolytic solution, we considered the effective dipole-dipole interaction between the QDs while undergoing diffusion. Figures 5(a) and (b) showed that the MSD and τ are not affected with the increase of QDs concentration (1-10 μM), for both the QD size cases, with respective interaction parameters being λ = 0.35 and 35. In ion channel forming aggregated state, each of the conductance state corresponds to the current burst across the bilayer and thus depicting an abrupt ion transduction pathway. As a general trend, it can be observed that when the conductance of the QD ion channel increases with the no. of aggregated QDs, the MSD drops in a sub-linear way. An aggregated structure formed by a larger sized QDs exhibits a six fold increase in the conductance value as compared to the former one. A larger aggregated structure as well as larger sized QDs respond weakly to the thermal agitation even though while characterizing definite ion transport pathways.
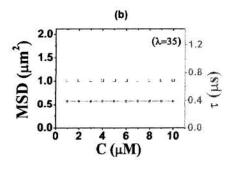
Fig. 5: MSD vs. concentration of QDs of diameters (a) 2 nm (b) 20 nm, in the electrolytic solution

As expected, the aggregation state of 2 nm QDs shows less undulation behavior (during current burst) (Fig. 6(a)) than a bare 2 nm QD in electrolytic solution. But, these aggregated structures show higher diffusive response than a bare 2 nm QD, in their pre-aggregated state, across the bilayer. On the other hand, the MSD of the conductance state due to the aggregation of 3 nos. of 12 nm QDs (Fig. 6(b)) exhibits nearly equal value (~1.7 μm²) with that of a bare 12 nm QD in the electrolytic solution (~1.68 μm²). But as it goes to the higher conductance states, the corresponding MSD values gradually decrease compared to the electrolytic environment. Note that, the relaxation time of an aggregated structure is higher or lower than the electrolytic solution and lipid bilayer in particular conductance states. It is observed that, the response time of an aggregated structure with 4 nos. of 2 nm sized QDs aggregation (Fig. 7 (a)) in a bilayer is close to that of the response of individual QDs in the electrolytic solution and the response time of 5 nos. of QDs aggregation (each QD of dia 12 nm) (Fig. 7 (b)) is similar to the response of independent QDs in their pre-aggregated state. This suggests that, as the size of the QD aggregated structure increases, their relaxation time is nearly equals to the time of a pre-aggregate structure while undergoing diffusion. Further, it is also clear that an aggregated structure with more no. of QDs move slowly from their equilibrium positions. Thus it is apparent that, the complex lipid bilayer environment has a control on the diffusion behavior of
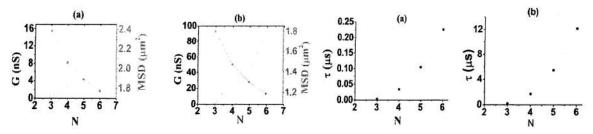

Fig. 6: Conductance state and MSD of QDs each of (a) dia. 2 nm (b) dia. 12 nm.
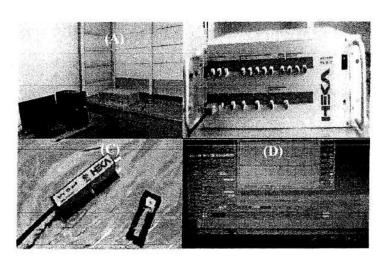
Fig. 7: Relaxation time vs. no. of aggregated QDs each of (a) dia. 2 nm (b) dia. 12 nm.

the aggregated structures created by the complete insertion of smaller sized (~2 nm) QDs into the bilayer. In this case, their thermal motion is restricted within the viscous lipid bilayer surrounding. Consequently, there is a significant reduction of the mobility in the media as compared to the electrolytic buffer environment. Alternatively, the aggregated structure formed by the partial insertion of larger sized (~12 nm) QDs is not greatly affected. This is due to the fact that, the aggregated structure may come in contact with a substantial volume of the electrolytic environment. In both the complete insertion as well as partial insertion cases, the high viscous nature of the bilayer would bind the bare QDs more tightly in the pre-aggregated state than in the aggregated state. Thus the thermal movement of the pre-aggregated QDs is significantly affected relative to the aggregated ones.

(2) Making Faraday cage, procurement and installation of electrophysiology setup

As mentioned above, mechanical as well as electrical stability of the lipid bilayer is very much critical in an ion channel experiment. The current fluctuation across a bilayer is very sensitive even to the slightest mechanical and

electromagnetic noise. Microscopic movements and vibrations present in all buildings can be damped out by an appropriate vibration isolation table placed at a suitable location. Different components such as, patch clamp amplifier main device, head stage and lipid bilayer setup were placed in a Faraday cage built on the table. The cage was connected to the building ground in order to suppress the electromagnetic noise. The side walls of the Faraday cage were draped by thick aluminum sheets. The electrophysiology setup along with patch master and fit master[®] data acquisition software was installed on a PC running on OS Windows 2007[®]. The following photograph shows the patch clamp set up along with Faraday cage, main amplifier and the computer interfacing.

(A) Ion channel recording setup (B) main amplifier (C) head stage pre-amplifier that connects electrolytic chamber and the main amplifier (D) monitor of PC displaying use of patchmaster software[®] laboratory

Year 3: (1) Synthesis and stabilization of CdSe and MnSe QDs

To use the QDs in biological application such as biosensing, biolabeling, bioimaging, it is very much important to understand the parameters that influence their optical properties significantly. In this section, we discuss preparation of high-quality CdSe QDs and their stabilization considering different factors such as, varying concentration of cadmium precursor, reaction time and aging etc. In addition, special emphasis was given to the study of pH dependent stability of CdSe QDs by considering natural media: the first, being citric media, (derived from lemon) and the other one is rose water. Similarly, we optimize the stability of WZ structure MnSe-TGA QDs by standardizing different factors, *viz.*, concentration of capping agent (TGA) and QDs precursor ratio (Mn^{2+}/Se^{2-}). In practice, cellular-biology experiments are generally conducted in a complex biological environment which contains a mixture of amino acids, salts, glucose and vitamins. Therefore, it is important to understand QD behavior under these environments for *in vitro* or *in vivo* studies. It is well-known that, bare nanoparticles tend to agglomerate immediately after being added to the culture media. In this regard, surface functionality along with the presence of some essential biological materials (such as, protein, serum, nutrients etc.) could help obtaining a stable dispersion of the QDs. In order to evaluate the QD dispersion in cell media, we considered study wrt media dependent optical response of MnSe-TGA QDs while bovine serum albumin (BSA) was used as a control dispersing agent. We have chosen BSA knowing that, serum albumin is the most abundant protein in blood plasma [25]. In addition, BSA has been widely used as a model protein for dispersing nanoparticles in physiological fluid [26,27]. We assessed commonly used cell culture media such as, Dulbecco's Modified Eagle Media (DMEM), Minimum Essential Medium (MEM) and Roswell Park Memorial Institute (RPMI).

Experimental Details

Synthesis of CdSe QDs: At first, 10% polyvinyl alcohol (PVA) solution was prepared by dissolving 10 g of PVA in 100 mL distilled water followed by stirring for 3 h. Then 0.62 g of cadmium nitrate-tetra hydrate [$Cd(NO_3)_2.4H_2O$] was dissolved in 100 mL of water followed by stirring for 20 min at 60°C temperature. 20 mL of 10% PVA was then added to Cd^{2+} solution during stirring process. The pH the solution was adjusted to 11 by adding sodium hydroxide (NaOH) in a drop wise manner. Next, 0.111g of selenium di-oxide (SeO_2) was added after sometime to the above solution followed by the addition of 0.1 g sodium borohydride ($NaBH_4$) as reductant. Finally, the mixture was subjected to stirring for 1 h at 100° C temperature. To examine the photostability of PVA dispersed CdSe QDs in natural media of varying pH, the QDs were dispersed in freshly prepared lemon water and in rose water. The pH of the undispersed CdSe-PVA (7.02), has changed to 3.42 and 7.42 in lemon and rose water media; respectively.

Synthesis of MnSe-TGA QDs: In a typical synthesis procedure, 0.62 g of manganese chloride-tetra hydrate ($MnCl_2.4H_2O$) and 0.11 g SeO_2 were dissolved in 22 mL distilled water followed by the addition of $NaBH_4$ of 0.1 g. Then, the pH of the solution was adjusted to 11 by adding NaOH in a drop wise manner followed by stirring for 5 min at 60°C temperature. Subsequently, 10% TGA was added to the above mixture. Finally, the solution was transferred to a teflon-lined stainless steel autoclave (of 50 mL capacity), and subjected to heat treatment at 180°C for 6 h, after the autoclave being sealed properly. Upon completion of the reaction in the liquid phase, the autoclave was allowed to cool down to room temperature naturally. The precursor extract was then subjected to centrifugation (~5,000 rpm) followed by filtration using a whatman® filter. The precipitate (residue) was washed with distilled water several times. In order to examine the photostability of the QDs in culture media, a series of experimental steps was employed following an earlier report [26]. According to this protocol, at first suitable amount of MnSe-TGA QDs was sonicated in DI water followed by the addition of BSA protein and finally, introduced in different cell media in separate petri-dishes. The samples were incubated at ~37°C, for about 6 h.

Results and discussion

For meaningful application in biological systems, all QDs need to pass through a series of stability and compatibility tests. It is essential to study the factors that have significant influence on their dimension, optical density and optical and emission characteristics. The samples of CdSe QDs of varying concentration ratio of Cd^{2+}/Se^{2-} 1:1,2:1,3:1,4:1 are defined as S_1,S_2,S_3,S_4; respectively. Whereas, the MnSe-TGA QD samples were prepared by varying TGA concentration (of 1, 5, 10%) and varying molar concentration of Mn^{2+}/Se^{2-} (of 2:1, 3:1, 4:1). We labeled the respective samples with TGA concentration of 1%, 5%, 10% as T_1,T_2,T_3 and Mn^{2+}/Se^{2-} molar ratios of 2:1, 3:1, 4:1 as M_1,M_2,M_3.

Effect of reactant concentration on the optical properties of CdSe QDs

Fig. 8(A) depicts the effect of Cd^{2+}/Se^{2-} precursor concentration on the UV-Vis spectra of CdSe QDs dispersed in PVA. In all the cases, the onset of absorption was found to be blue shifted from the bulk value (λ_{onset}~716 nm). This implies effective quantum confinement of the charge carriers in the QDs. The samples (S_3, S_4) with higher Cd^{2+} concentration exhibit strong 1s-1s excitonic absorption at λ_{ex}=310 nm. A low concentration of Cd^{2+} leads to the featureless characteristics with long tailing, depicting inhomogeneity in the samples. Our results indicate the more
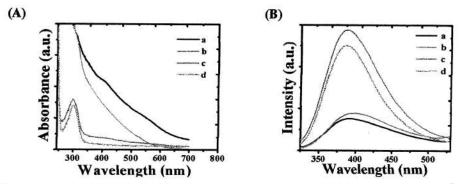

Fig. 8: (A) UV-Visible and (B) PL spectra of CdSe QDs derived from precursors of Cd^{2+}/Se^{2-} ratio (a) 1:1 (b) 2:1 (c) 3:1 (d) 4:1

likely formation of smaller sized QDs in precursors that are rich in Cd^{2+}. It may be due to the fact that, a proportionately larger concentration of Cd^{2+} ions (as compared to Se^{2-} ions) could provide a substantial number of nucleating sites for the growth of CdSe QDs. Consequently, a larger number of nucleation sites at a given concentration of Se^{2-} precursor would lead to the formation of smaller sized QDs [28]. The large no. of nucleation sites around the Cd^{2+} ions is due to the smaller ionic radii of Cd^{2+} ions (~109 pm) compared to the Se^{2-} ions (~184 pm).

Referring to Fig. 8(B), the PL spectra of QDs are found to comprise of two emission peaks: due to band-edge (λ_{BE}) and defect related (λ_{DE}) emissions. The λ_{BE} was found to be located at ~380 nm with a FWHM ~ 65 nm. The λ_{DE} was in the range of 415-428 nm for QDs derived from varying Cd^{2+}/Se^{2-} ratios (1:1 to 4:1). The observed defect related emission response is attributed to the radiative transitions mediated via surface trap states. The states are created by entrapped electrons inside a selenium vacancy with holes in the valence band [29]. As observed from the PL spectra, the dominant response of the defect related emission over the band edge emission, in samples S_1 and S_2, signifies inadequate surface passivation of the QDs. Previously, a lower Cd^{2+} concentration was found to be insufficient for effective dispersion in PVA [30]. In our case, the intense band edge emissions, for S_3 and S_4, are due to significant passivation of surface defects. A higher concentration of Cd^{2+} would realize insufficient PVA for effective capping [28] and that is why we observed reduced band edge-to-defect related emission for S_4 as compared to S_3. As the effect of the reactant concentration has provided the best quality sample for $[Cd^{2+}]/[Se^{2-}] = 3:1$ (S_3) we opted for studying the effect of reaction time, pH and aging effect of the aforesaid precursor.

Effect of reaction time on the optical properties of CdSe QDs

Fig. 9(A) and 9(B) show the dependence of absorption and emission properties of PVA dispersed QDs with reaction time for a fixed Cd^{2+} concentration. Up to 30 min. of reaction, only featureless characteristics were observed revealing thereby no excitonic absorption. A sharp absorption response was observed at ~ 328 nm when the reaction was allowed for 60 min and beyond. Since the position of the absorption maxima did not change with time, the average size of the QDs is expected to be nearly uniform. Previously, it was argued that, PVA matrix could restrict the growth of the particles and therefore, the growth process becomes homeostatic [28].
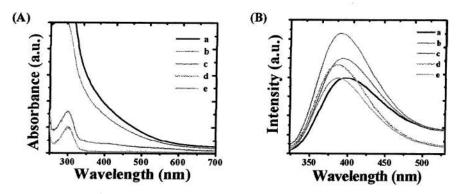

Fig. 9: (A) UV-Visible and (B) PL spectra of CdSe QDs prepared with a reaction time of (a) 10 (b) 30 (c) 60 (d) 90 (e) 120 min.

The photoluminescence response of the CdSe-QDs depicts asymmetrically stretched spectra, as shown in Fig. 9(B). Upon deconvolution (not shown), the λ_{BE} is found to be located at ~380 nm while λ_{DE} at ~417 nm, when the reaction time was varied in the range of 10-120 min. Although, defect related emission was prominent for samples prepared under a smaller reaction time environment, the overall PL emission was found to be strongest for the sample prepared under a 60 min. of time duration. For an increased reaction time, there is a possibility of collective assimilation of nanocrystallites leading to suppressed emission response. In contrast, an insufficient reaction time could lead to the unsaturated bonding between Cd^{2+} and Se^{2-} ions. In our study, a 60 min. of reaction time was found to ensure a sharp exciton absorption and intense emission response.

10

Effect of pH dependent media and aging

The typical absorption and emission behavior of CdSe-QDs dispersed in different pH media are shown in Fig.10 (A) and Fig.10 (B); respectively. As can be observed from the absorption spectra, the exciton absorption is found to be located at ~300 nm (~ 4.13 eV) for neutral PVA as well as acidic media. However, the characteristic excitonic feature is relatively broader for the acidic media than the neutral one. A relatively broad size distribution might have led to a broadened peak in the acidic media. The response of alkaline media is characterized by a significantly red shift (~0.76 eV) of the exciton absorption along with broad absorption feature.
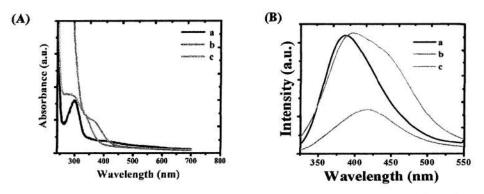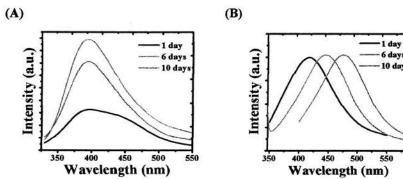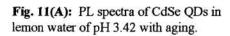
(A)   **(B)**

Fig. 10 (A): UV-Visible and (B) PL spectra of CdSe QDs in (a) PVA, (b) rose water, and in (c) lemon water

Fig. 10(B) signifies the PL response of the QDs dispersed in the lemon water, PVA and rose water media. Here, band-to-band emission (λ_{BE}) peak is located at ~380 nm for both the cases, while the λ_{DE} maxima are positioned at ~430 nm and ~ 416 nm in lemon water and PVA media; respectively. Note that, the defect-related emission intensity is predominantly high in case of acidic media over the other environment. Interestingly, the QDs in alkaline media exhibited the suppressed emission response. Because of the improved defect related emission behavior in lemon water, the emission response of the QDs becomes more asymmetric as compared to others.

Fig. 11 depicts a set of spectra highlighting results with regard to stability of the QDs due to independent aging effect in respective media. As shown in Fig.11(A), the near band edge emission (NBE) gets improved by a factor of ~ 4 when the specimen was subjected to aging for days in lemon water. However, the exessive aging effect did not show further improvement. As can be found, the emission response is suppressed (by a factor of ~2.7) when the specimen was aged for 10 days. However, as can be found from Fig.11(B), CdSe QDs in rose water exhibited red shifting (from λ=416 to 475 nm; E_g=2.98 to 2.61 eV) of the emission peak with the corresponding aging effect. The red shifting can be ascribed to the size effect owing to coalesce of QDs. Interestingly, though a peak-shift was evident with aging, the overall emission intensity remained uniform for all the specimens. Fig 11(C) depicts a comprehensive view of the QD stability due consideration of the aging effect in different media.

(A) **(B)** **(C)**

Fig. 11(A): PL spectra of CdSe QDs in lemon water of pH 3.42 with aging.
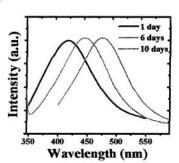
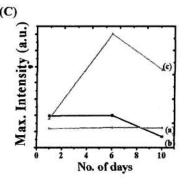**Fig. 11(B):** PL spectra of CdSe QDs in rose water of pH 7.42 with aging.

Fig. 11(C): Maximum intensity vs. no. of days CdSe QDs in different media
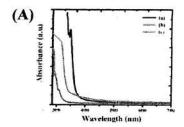
In rose water environment, the NBE intensity remained constant with aging. However, in PVA media, the NBE intensity of the QDs does not change substantially up to 6 days. There is drastic reduction of NBE for 10 days of aging. In contrast, the intensity gets significantly enhanced in lemon water for 6 days of aging beyond which a slow decay was realized. The probable reason for a higher stability of the QDs in lemon water media is attributed to the esterification of PVA to PVA-C in presence of citric acid ($C_6H_8O_7$) contained in the lemon water [31].
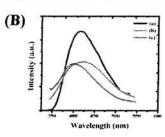
As far as QDs stability is concerned, the carboxyl-functionalized PVA host provides a better environment over the untreated PVA. This is because of the availability of an ample amount of free Cd^{2+} ions that are capable of imparting charge balancing with carboxylate (COO⁻) ions. Consequently, it results in a more stable colloidal system. This modified PVA is reasonably less cytotoxic, and therefore attractive for cellular studies. On the other hand, in basic medium (QDs in rose water), because of the presence of geraniol in the rose oil the PVA-rose water mixture becomes superhydrophobic in nature [32]. This superhydrophobic oil -in -water system behaves as a miceller based microreactor system. Consequently, there is a high probability that QDs would come close to each other and coalesce outside these micro-reactors. This is the reason why we observed a red shift in the emission spectra and larger FWHM in DLS studies.
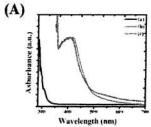
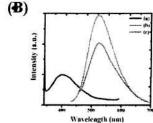**Effect of TGA concentration on the optical properties of MnSe QDs**
Figure 12(A) depicts the effect of TGA concentration on the optical absorption spectra of MnSe-TGA QDs. As shown, prominent absorption edge was found to be located at ~303 nm (E_g ~4.09 eV) in case of sample T_3 (curve c). This implies effective quantum confinement of the charge carriers in the QDs which is characterized by a blue-shift of ~0.5 eV from the bulk value (E_g~3.5 eV) of the ZB-MnSe system [33-36]. In contrast, a slight blue shifting of ~0.07 eV and significant red shifting of ~0.8 eV were observed for samples T_2 (curve b) and T_1 (curve a); respectively. It is worth mentioning here that, the blue shift observed are small and in the range of ~0.07-0.5 eV, for samples T_2 and T_3. This is due to highly localized nature of 3d electronic bands of Mn atoms. Correspondingly, the quantum confinement induced by cordially bonded organic layers would lead to a much smaller change in these bands [36].

The corresponding photoluminescence (PL) spectra of the QDs (T_1, T_2, T_3) under an excitation wavelength of ~300 nm, are shown in Figure 12(B). Each of the emission spectra were deconvoluted to uncover different peak positions. Upon de-convolution, it was observed that, the λ_{BE} of the samples T_2 and T_3 and located at ~397 nm

Fig. 12: (A) UV-Visible and (B) PL spectra of MnSe-TGA QDs prepared with different TGA concentrations of (a) 1% (T_1) (b) 5% (T_2) (c) 10 % (T_3), for a fixed Mn^{2+}/Se^{2-} =2:1.

Fig. 13: (A) Absorption and (B) PL spectra of MnSe-TGA (TGA: 10%) QDs with different Mn^{2+}/Se^{2-} ratios of (a) 2:1 (M_1) (b) 3:1 (M_2), and (c) 4:1(M_3).

and ~ 400 nm, resemble closely with the band emission peak (~364 nm) of the ZB type MnSe system [37]. Whereas, λ_{BE} positions were red shifted to ~ 406 nm, in case of T_1. The λ_{DE} was observed to be in the range of 461-459 nm for QDs samples T_1 to T_3. The defect related emission peak may have arisen from the defects in the metastable WZ nanocrystal core [38]. Note that, QDs of T_1 sample has band edge emission response slightly weaker than T_3. In contrast, a dominant defect related emission was noticeable for T_2 as compared to T_3.

The dominant feature of the defect related emission over the band edge emission, in sample T_2 may signify inadequate surface passivation of the QDs. On the other hand, intense and symmetric band edge emission is evident due to significant passivation of the surface defects in the metastable WZ QDs with a higher concentration of capping agent TGA (T_3).

12

Effect of precursor concentration on the optical properties of MnSe QDs

Figure 13(A) and (B) represent the dependence of absorption and emission behavior of MnSe QDs (coated with 10% TGA) for different precursor concentration ratios (Mn^{2+}/Se^{2-}). The sample M_1 (Figure 13(A), curve a), exhibits a strong excitonic absorption feature at ~303 nm (~E_g=4.09 eV). Whereas, a significant red shifting (~ΔE=1.03 eV) of the exciton peak was observed at λ~408 nm (E_g=3.03 eV) with an increasing value of the precursor ratio (M_2, curve b and M_3, curve c). Note that, the band gap of sample M_1 is slightly blue shifted (~0.5 eV) wrt the bulk value of ZB MnSe (E_g=3.5 eV) system, but is apparently larger with respect to RS type MnSe (E_g=2.5 eV) system. In contrast, the sample M_2 and M_3 as obtained with a higher Mn^{2+} concentration showed an adequate blue shift (~0.5 eV) with respect to the bulk RS structure. This may suggest that, with the incorporation of an excess Mn^{2+} concentration there can be a partial phase change of WZ structure of MnSe QDs to RS one [39].

The PL responses of MnSe QDs with different Mn^{2+}/Se^{2-} precursor ratios are depicted in Figure 13(B). The spectrum recorded for sample M_1 (curve a) exhibits band edge emission (λ_{BE}) at ~400 nm [37] and surface defect related emission (λ_{DE}) at ~459 nm [38]. Conversely, intense emission bands were observed at ~515 nm and ~517 nm as for samples M_2 (curve b) and M_3 (curve c); respectively. The PL emission intensity of the M_3 sample is approximately halved as compared to the M_2 sample. The de-convolution of asymmetric PL spectra have revealed other emission peaks located at ~554 nm and ~566 nm; for M_2 and M_3 samples; respectively. These emission bands are ascribed to the $3d$ electron transitions of Mn^{2+} [36]. A lowered emission intensity by a factor of ~1.18 in case of M_3 sample over the M_2 one is probably due to the interaction of the neighboring Mn^{2+} ions at the nearest, the second nearest, and at the third nearest neighbor-sites with an increase of Mn^{2+} concentration [39].

Dispersion and stability optimization of MnSe-TGA QDs in cell culture media

The optical and colloidal stability of the fluorescent particles in different chemical environment are also important prerequisites for their application in biolabeling and biosensing. As mentioned earlier, different dispersing agents like BSA protein influence significantly as for the stability of the QDs in biological environment. We have made a comparative study on the stability of MnSe-TGA QDs in different dispersion media by considering both presence and absence of the dispersing agent (BSA protein). Figure 14(A) demonstrates that, without addition of the dispersing agent (BSA), excitonic absorption peak of MnSe-TGA QDs in PBS remains constant (~303 nm) as we have observed in DD media. Whereas, they were significantly red shifted to ~313, ~321 and ~329 nm when dispersed in DMEM, MEM and RPMI media; respectively. This clearly indicates the aggregation of QDs in these media. In cell media, high ionic strength results in dominant van-der Waal attraction over electrostatic repulsive behavior leading to agglomerated structures [40]. In contrast, a nearly stable dispersion of the MnSe-TGA QDs in culture media has been observed upon addition of BSA. The exciton absorption peak remained unaffected in (~303

(A)   **(B)**   **(C)**

Fig. 14: (A) UV-Visible and (B) PL spectra of MnSe-TGA (TGA 10 %, Mn^{2+}/Se^{2-}= 2:1) QDs in different dispersing media in presence and in absence of dispersing agent BSA. Figure (C) depicts aging effect on NBE of MnSe-TGA QDs (prepared with TGA:10% and Mn^{2+}/Se^{2-} =2:1) with BSA as a dispersing agent.

nm) in PBS as well as in DMEM media. Whereas, it is slightly (~308 nm) and significantly (~327 nm) red-shifted in MEM and RPMI media; respectively. The enhanced emission response of the QDs with BSA dispersion signifies an improvement of the QD stability, as compared to the QDs dispersed directly in the cell culture media (Fig. 14(B)). Nevertheless, in presence of BSA proteins, MnSe-TGA QDs in DMEM and MEM media exhibited

stronger PL responses over RPMI. This suggests effective absorption of BSA molecules on the MnSe-TGA QD surfaces in DMEM and MEM.

Figure 14(C) depict a number of PL spectra highlighting studies with regard to stability of the QDs upon BSA dispersion due to independent aging effect in different cell culture media. We can invoke that, MnSe-TGA QDs are more stable in DMEM (in 3 days of aging) and MEM media (in 5 days of aging) than RPMI cell culture media. A greater stability of PVA coated SPION and BSA coated TiO_2 particles in DMEM media over RPMI media were also predicted in earlier works [40-41]. Note that, in DMEM and MEM media, the presence of a larger amount of divalent cations (Ca^{2+}, Mg^{2+}) as compared to RPMI media can act as an effective bridge to bind negatively charged BSA molecules to negatively charged MnSe-TGA QDs [40]. In contrast, a proportionately higher concentration of phosphate ions, in RPMI media, than those of other cell media, is likely to compete with BSA molecules so as to adsorb into the QD surfaces resulting in instability. As shown by Boonsongrit et al, nearly 70% of BSA was found to release from hydroxyapatite microspheres, in half an hour, in the presence of 10 mM phosphate [42].

(2) Micropore formation using various methods

There are a number of different techniques such as, laser ablation [43], ion beam [15], and spark assisted (SA with and without chemical engraving) [44] that can be employed to create micropores in selectively chosen substrate materials. The purpose of a micropore based substrate is to use in planar chip technology.
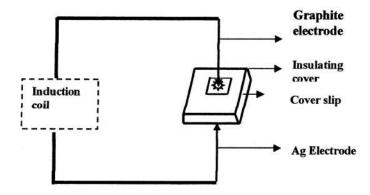
Spark assisted method

Among these, the SA method is generally employed owing to its cost-effectiveness and simplicity in design/assembly. In fact, we made an attempt to create micropores in the 150 μm thick chip which could be used as a substrate material. The schematic of the set-up used for the SA method is shown in Fig. 15(a).

Materials used in the experiments are

(i) Induction coil (Model 25 M.M.SPARK) which was used to maintain a high voltage across the electrodes.

(ii) Electrically insulating coverage around the cover slip that separates two electrodes

(iii) Two needle shaped electrodes: one of graphite (tip diameter 500 μm) and other of silver (tip diameter 500 μm).

(iv) One screw gauge (least count: 0.01 mm, Mitutoyo Co.) for adjusting the air gap between the two electrodes.

First, all the components were kept on a vibration free table. With the help of a screw gauge an air gap (~10 μm) is established between the two electrodes along a vertical configuration. The surrounding area of the chip was made insulated with an insulating cover to minimize the scattering. The electrodes were subjected to 12 V DC supply with the help of an induction coil (~12V) that could generate high voltage spark across the tips of the electrodes leading to an aperture on the substrate. Fig. 15(b) shows a typical micrograph of the micropore formed on the borosilicate glass substrate. A surface polished, nearly spherical, ~10 μm dia pore was witnessed from the SEM image. Unfortunately, pores of this size could be efficiently used in cell studies [19] but not adequate to support planar lipid bilayers. Our experimental setup did not allow to obtain larger sized pores, though it was reported earlier that with the application of a high voltage of ~30 V, pores of diameter ~300 μm could be achieved [44].
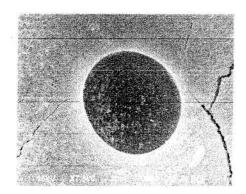

Fig. 15: (a) Schematic of the spark assisted setup for creating micropore, b) SEM image of a SA micropore (dia~10 μm)

Laser drill method

Micropore formation by laser drilled method was carried out at Laser Biomedical Applications & Instrumentation Division, Raja Ramanna Centre for Advanced Technology, Indore. Fluorine laser mask projection has been used to micro-machine the holes in different materials namely glass cover slip, PMMA, cellulose acetate and polyimide. Glass cover slip is coated with NOA 61 UV epoxy on both sides and holes were ablated in UV epoxy under 157 nm irradiation at 6.4X with 22 mJ pulse energy (455 mJ/cm^2 fluence) at 50Hz for 25 s (integrated power density 570 J/cm^2) till the UV epoxy has been completely removed on both sides thus exposing a circular aperture in the glass cover slip. This has then been etched using 20% HF acid solution for 20 minutes thus creating a through hole in 150 micron thick cover slip.

The 1 mm thick PMMA sample was ablated under 157 nm mask projection and took 250s at 100 Hz. The 100 μm thick cellulose acetate sample was also ablated under 157 nm mask projection and took 220s at 100 Hz while the 60 μm thick polyimide sample took 50s at 100Hz. All laser drilled apertures are shown in Fig. 16.

Fig. 16: (a) 160 μm hole in borosilicate glass coverslip, b) 80 μm hole in PMMA, c) 100 μm hole in cellulose acetate, and d) 110 μm hole in polyimide

(3) Formation of lecithin bilayer and QDs induced ion channel using planar chip technology

The lipid bilayer experiment was performed using a 100 μm thick cellulose acetate substrate that has a centrally located aperture of dia ~100 μm. The cellulose acetate system was chosen as it possesses good electrical properties (low dielectric constant, low dielectric loss), good thermal properties along with high values of elastic modulii that are comparable to the values observed for other polymeric materials (Teflon, PP, PET) generally used for this type of applications. A substrate, having a good mechanical and thermal stability, is capable of supporting a very stable bilayer. In addition, the substrate material with low dielectric constant and dielectric loss can contribute only weakly to the effective capacitance and thus may help even in the detection of single ion channel events. In a

15

typical ion channel experiment, the preferred diameter of the aperture is in the range of ~80-100 µm [45]. Shown in Fig. 16(c), is an aperture (of diameter d_a= 100 µm) located at the center of the cellulose acetate substrate, which was developed by using a femto-second KrF excimer laser available at RRCAT, Indore. In real cells, phospholipids are the key elements of a bilayer membrane which regulates the flow of ions and other important molecules for cellular activity. Knowing that lecithin is a major source of phospholipids available in nature, we intended to work with bilayer derived from lecithin. In order to obtain a lecithin bilayer, we considered soy lecithin which was extracted from soya-been seed (model RKS-18) through solvent extraction process followed by water degumming process [46,47].

The complete ion channel experiment was performed using a patch-clamp amplifier (EPC10) and patchmaster software (HEKA Elektronik, Germany)®. The main amplifier had an extension called the head-stage which was capable of interfacing amplifier and the planar chip components. The head-stage was connected to Ag/AgCl electrodes for the data acquisition of single ion channels across the lipid bilayer (Fig. 17). A lecithin lipid bilayer membrane was formed around the aperture by a painting method
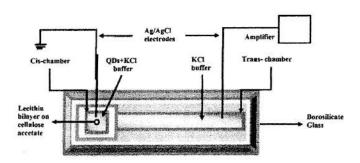

Fig. 17: Schematic of a typical ion channel measurement setup showing different components

following an established procedure (Montal-Müeller technique) [48]. The impermeable bilayer acts as a partition between the two compartments (cis and trans- chambers) containing electrolytic buffer (1 mL of 1M KCl, 10 mM HEPES, at pH= 7.5 and at room temperature). As mentioned above, the compartments were connected to the patch clamp amplifier via a pair of Ag/AgCl electrodes prepared in 0.5 M KCl (Fig. 17). The resulting currents were filtered by a low-pass filter (with a four-pole Bessel filter at 1 kHz, with a sampling frequency of 10 kHz by a computer with an analog-to-digital converter). In order to suppress electromagnetic noise, the whole setup was kept in a Faraday cage with ground connected to the building ground. The amplified current was monitored in a PC working on OS windows 2007® using the patchmaster software®.

Evidence of formation of a stable lecithin bilayer around the aperture
The bilayer capacitance is given by: $C_m = I/(dV/dt)$ [49]. Here, I is the measured current across the bilayer in response to an applied voltage ramp dV/dt. In the present case, 100 mV was applied for 20 ms giving out a ramp of dV/dt =5 V/s. As can be found in Fig. 18, the membrane current was found to be ~209.5 pA for which several traces were collected in order to ensure the bilayer stability with lapse of time. The estimated (lecithin) bilayer membrane capacitance was found to be ~42 pF. Theoretically, lecithin membrane capacitance was predicted as ~57 pF through using the following relation [15]:

$$C_m = C_s \frac{\pi}{4} d_p^2 \tag{17}$$

where, C_s is the specific capacitance of soya-lecithin bilayer (~0.75 µF/cm^2) [50]. While forming a stable bilayer, the whole aperture was believed to be covered by the bilayer itself. In that case, the diameter of the aperture (d_a) is equal to the membrane diameter (d_p). Again, in planar lipid bilayer experiment, the membrane capacitance (C_m) and the diameter (d_p) of the membrane carrying micro-pore are related as,

$$C_m = \frac{\varepsilon_0 \varepsilon_r A}{d}. \tag{18}$$

16

Here, $A = \frac{\pi}{4} d_p^2$ is the area of the membrane, ε_0 is the permittivity of the free space (ε_0=8.85x10^{-12} F/m), ε_r is the dielectric constant of the membrane and d is the thickness of the lipid bilayer. Considering ε_r of lecithin equals to the dielectric constant of the supported lipid bilayer in the aqueous solution (ε_r=3) [51], the lecithin bilayer thickness is calculated as ~4.96 nm. The bilayer under study was found to form a giga seal (~3-10 GΩ) and the bilayer was fairly stable up to a time duration of 390 s. The stability of the bilayer can be assessed from a fairly constant value of membrane current (~209 pA), recorded at different times (Fig. 18).
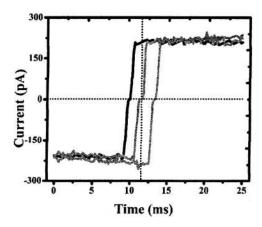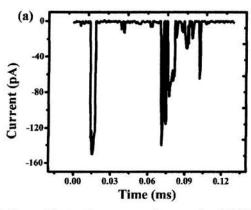

Fig. 18: Variation of current with the application of a ramp voltage in the lecithin bilayer, recorded at different times

QD induced ion channel response, nanopore formation and theoretical assessment

After obtaining a stable bilayer around the aperture, 4.2 nmol/ml water soluble CdSe QDs (~20 nm) were injected into the cis- compartment of the electrolytic chamber with the help of a Hamilton® microsyringe. Note that, while trans- side of the chamber was connected to the head stage of the amplifier, the cis- compartment was held at virtual ground. The noise level of the whole setup was reduced to < 2 pA by grounding the Faraday cage with the ground of the building. About a minute later the QDs were added, current bursts were observed in response to an applied voltage across the lecithin bilayer membrane. Fig. 6 depicts the traces of current fluctuation when the bilayer was subjected to two different biasing voltages of -10 mV (Fig. 19(a)) and -20 mV (Fig. 19(b)). An apparently enhanced current magnitude was witnessed with an increasing biasing voltage.

We anticipate instant oligomeric aggregation of QDs in the lecithin bilayer, allowing counter ions to pass through the nanopores under an external field. A higher voltage indeed facilitates a higher concentration of ions resulting in a higher magnitude of the current burst. The plots representing a number of events vs. current histograms over a number of experiments are shown in Fig. 20. As can be found, there exist two dominant conductance states: a high-end level of ~14.3 nS and a low-end one as ~6.3 nS (inset of Fig. 20(a)), corresponding to the bias voltage of -10 mV.

The respective conductance levels, corresponding to a higher bias voltage (-20 mV), are ~21.1 nS and 11 nS (inset of Fig. 20(b)). Earlier, a prime conductance value of ~2.3 nS was observed by an earlier group where ~12 nm CdSe QDs were inserted in an artificial phospholipid bilayer [21]. Moreover, the high-end value (~14.3 nS) is close to the conductance value ~15.8 nS, as predicted theoretically for ion channels created by 12 nm CdSe QDs and reported in an earlier work [52]. The dwell time, which signifies the duration of on/off condition of a particular conductance state, as a result of ion channel activity can be estimated by averaging over a number of events. In the present case, the magnitude of dwell times are estimated to be 384, 400 μs and 390, 411 μs, as for -10 mV and -20 mV bias voltage cases; respectively. Know that, the conductance value is the intrinsic parameter of a definite ion channel and is solely dependent on the interface region of the nanopore created by QDs in aggregate form. As far as the interface region is concerned, there can be two possibilities of well-defined nanopore geometry: formation of spherical and non-spherical nanopores. For mathematical simplicity, generally spherical nanopores are treated without any curvature effect. Non-spherical nanopores involve complicated formula but better suited for a large aggregation number. Presuming the ion mobility uniform throughout the experimental chamber, here we discuss *both the approximations to adjudge our experimental results.*

17

Fig. 19: Current fluctuation measured across the lipid bilayer due to insertion of QDs at a biasing voltage of (a) -10 mV (b) -20 mV

Fig. 20: Event vs. current histograms of QD induced ion channels, corresponding to the bias voltages (a) -10 mV (b) -20 mV. The figure-insets showing the respective conductance-histograms for identifying individual open conductance states, away from the closed states.

Model 1: Ion channel activity due to spherical nanopores

This is an oversimplified version of the entrapped region created by spherical QDs. In this case, the conductance level G_s can be related to the spherical- shaped nanopore of size d_{spore} as [21]:

$$G_s = \sigma \frac{\pi d_{pore}^2}{4D}. \tag{19}$$

Here, D is the diameter of the QDs forming the aggregated structure, σ is the conductivity of the electrolytic buffer. The conductivity of the 1 M KCl+10 mM HEPES buffer at 300 K is ~98 mS/cm, whereas size of the CdSe QDs used in the experiment was ~20 nm.

Model 2: Ion channel activity due to non-spherical nanopores

Pores of non-spherical geometry are mostly considered due to insertion of helical proteins in cell-membranes leading to ion channels. We can also use the relevant formula in the present case, owing to the curved surfaces of the QDs and knowing that, the aggregated system is far from equilibrium. Since the pores are created by aggregation of QDs with curved surfaces, in reality, one cannot expect formation of spherically symmetric

entrapped regions (spherical nanopores). In that case, ion channel conductance (G_{ns}) in a bilayer membrane can be related to the diameter of the QD-induced nonspherical pore as per the following relation [52-54]

$$G_{ns} = \frac{\sigma l \pi d_{nspore}^2}{\left[4(l + \pi d_{nspore}/4)\right]} \qquad (20)$$

Here, l is the length of the pore and σ being the conductivity of the buffer. In our case, l= 4.96 nm which is the thickness of the lecithin membrane; d_{nspore} is the diameter of the non-spherical pore formed by the QDs.

Referring to model-1, and considering two conductance values of ~6.3 nS and 14.3 nS (corresponding to a bias voltage -10 mV), we predict the size (d_{spore}) of the spherical nanopores as ~4 nm and ~6.09 nm. The corresponding pore diameters, as calculated using model-2 and applicable for the non-spherical nanopores (d_{nspore}), were estimated to be ~0.95 nm and ~1.5 nm. Apparently, $d_{nspore} < d_{spore}$. As for the case of the biasing voltage of -20 mV, the respective pore diameters of the spherical nanopores were observed to be ~5.3 nm and ~7.5 nm that corresponded to the conductance levels of 11 nS and 21.1 nS; respectively. The non-spherical pores, are however, characterized by a smaller dimension of ~1.22 nm and ~1.8 nm in these cases.

It is likely that non-spherical pore formation is a better approximation which could account for interfacial effects and possible surface charge interactions among neighbouring QDs. The consideration of non-spherical pores over spherical ones was also realized in a similar work [55]. Not surprisingly, the ion channels induced by the QDs can be dependent on the shape of the nanopores, which may be due to non-static nature of the aggregated QDs. Previously, nanpore shape- dependent ion conductance response was noticed for KasA potassium channels [55]. It was believed that, when the bilayer is subjected to a biasing field, QDs permeate and aggregate owing to a net dipole moment of the dots [23]. However, the formation of nanopore is a transient process and may be affected by thermal effect and a stress fluctuation. In presence of an external electric field, the QD with a dipole moment experiences a torque thus enforcing its insertion into the membrane. The aggregation behavior of QDs is believed to be due to the dominance of electrostatic interaction of dots over Brownian agitation resulting in a conformation of minimum surface energy.

As stated above, the variance of pore conductance strictly depends on the shape of the pore as well as on the diameter of specific nanopore. More precisely, the pores are created by the transient aggregation of the QDs, creating current bursts of varied magnitudes. Now both the models can be used independently to compute the number of QDs (N) involved in the creation of an aggregated structure, described by the following relation [23]:

$$d_{spore}, d_{nspore} = D_{dot}\left[1/Sin(180/N) - 1\right] \qquad (21)$$

The spherical shaped nanopores, exhibiting high (14.3 nS) and low (6.3 nS) values of conductance states are as a result of aggregation of 3.6 and 3 nos. of QDs; respectively. The corresponding N values were 2.6 and 2.4, for non-spherical pores. It is worth mentioning here that, a coplanar assimilation of ~3 QDs would represent the most close-packed network and ions are not necessarily allowed should the pores are filled with lipid molecules. It is very likely that, the migration of ions through nanopores is highly stochastic in nature, but capable of forming most probable ion conductance states owing to activity of transient pores. This is because an aggregation number $N < 3$ has no physical meaning, as far as the entrapped region is concerned. But, an aggregation of 3 QDs would represent a minimum energy configuration, that might describe a small, open conductance state when ions make their way for free passage, in response to a biasing voltage of -10 mV. In contrast, in a spherical nanopore approximation (model-1) an aggregation of ~3.6 QDs would indicate momentary involvement of an extra quantum dot in the aggregated state, giving rise to the formation of a larger nanopore, and consequently a higher conductance level. On the other hand, number of aggregated QDs corresponding to the conductance values of 11 nS and 21.1 nS (corresponding to a gating voltage -20 mV) are found to be 3.4 and 3.9; respectively. In contrast, with reference to model-2 (non-spherical pores), the relevant conductance states are characterized by an aggregation no. of 2.55 and 2.7.

Owing to consideration of larger sized QDs, we observed that the spherical pore diameter created by the QDs are comparatively larger than those reported by other groups [21, 23]. Theoretically, an aggregation of 5, 6 QDs may be possible, but in reality, thermal agitation is likely to perturb such a configuration for a longer duration of time [56]. As a consequence, it can flip either to 3 or, nearly 4 QD aggregation exhibiting a minimum energy configuration that is thermodynamically favorable. The undulation of QD aggregation may also be responsible for this flipping action. It is possible that QDs which experience oligomeric aggregation, would depart from their exact positions with time. As a result, channel events may exhibit stochastic trend due to the dynamic nature of ion

conducting pathways (nanopores). But the most probable states can be ascertained through histogram plots on a number of channel events and using the relevant theory of nanopores. We also invoke that, the observation of two conductance states, for a given biasing voltage may not represent independent ones but may call for simultaneous opening of an independent state. In this regard, mixed states due to simultaneous opening of fundamental states need to be addressed, which is in progress. It may be noted that, the ion channels could not be recorded at a higher biasing voltage owing to bilayer instability causing large leakage current.

10. Detailed analysis of results indicating contributions made towards increasing the state of knowledge in the subject:
~Given the design consideration of our electrophysiology setup, the major contribution being QD induced current fluctuation across an artificial bilayer. Although spherical and nonspherical nanopore formation can be possible theoretically, our experimental results predict stochastic nature of these nanopores. Synthesis and characterization of surface functionalized QDs, formation of stable bilayers around an aperture, and recording and analysis of current bursts have been detailed in # 9.

11. Conclusions summarizing the achievements and indication of scope for future work

- An electrolytic chamber of working area ~1.76 cm^2 (spherical region of dia. ~1.5cm) and substrate thickness ~150 μm can be helpful for effective electrophysiology recording. A reduced dissipation factor, low effective capacitance combined with high mechanical stability would make glass and quartz as the suitable candidates for planar chip architecture.

- From a theoretical modeling on Brownian aspects QDs, we predict that, in the pre-aggregated state, owing to a higher relaxation time experienced by smaller sized QDs (~2 nm) they tend to localize across the bilayer more tightly as compared to the QDs of larger size (~20 nm). Moreover, an aggregated structure is found to be more diffusive than a bare QD in the pre-aggregated state. The relaxation time gets increased by a factor of ~56 and ~64 folds as for the highest (6 QDs aggregation) conductance state than the lowest state (3 QDs aggregation) for ion channels created by a respective aggregation of ~2 and 12 nm sized QDs. Consequently, the response time of the conductance states of the ion channel formed by the larger sized QDs (τ_{12}) is ~50 times larger than the states created by smaller sized QDs (τ_2). It also provided with the highest conductance and MSD of ~92.31 μS and ~1.18 μm^2; respectively. In addition, the relaxation time of the aggregated structure aroused due to the 4 nos. (each QD of size ~2 nm) and 5 nos. of QDs (each of QD size ~12 nm) were found to be nearly equal to those of the bare QDs in the electrolytic solution and the pre-aggregated state in the lipid bilayer; respectively. Understanding the dynamics of QDs while making their ways through the semi-permeable bilayer membranes would find immense scope while considering specific ion channel regulation and manipulation for therapeutic applications including targeted drug delivery.

-We demonstrated the evolution of optical response of CdSe QDs in natural media: citric and rose water environment. In terms of stability, the QDs in lemon water has a better optical response than rose water media. The injection of carboxyl (-COOH) functional group with the PVA is provided by the esterification of PVA to PVA-C in the citric acid media. In rose water media, because of the presence of geraniol in the rose oil the PVA-rose water mixure becomes superhydrophobic in nature. This superhydrophobic oil -in -water system behaves as a miceller based microreactor system. Consequently, there is a high probability that QDs would come close to each other and coalesce outside these microreactors.
We have also studied the dispersing media dependent stability of MnSe-TGA QDs by using BSA as dispersing agent. Addition of BSA as dispersing agent significantly improves the QDs dispersion in DMEM and MEM over RPMI media. The variation of stability in different cell culture media was found to largely depend on different interaction mechanism in the respective media. MnSe being fluorescent and magnetic can have immense potential in biophysical applications where iron based systems can be adequately replaced by MnSe particles within a permissible limit.

-The synthesized QDs exhibited voltage dependent current fluctuations across the reconstituted soy-extracted lecithin bilayer supported on a cellulose acetate substrate. A higher biasing voltage is expected to facilitate migration of a higher concentration of ions, thereby exhibiting a higher current fluctuation. The ion channels

were believed to be caused by the passage of ions through entrapped regions of the QD aggregates (nanopores). The number of QDs, responsible for creating a conductance state was found to vary with the model-type, and characterized by different nanopore size. As a general trend, non-spherical nanopores with a smaller diameter, could exhibit similar ion conductance pathways as the case for the spherical nanopores with a larger diameter. Referring to spherical nanopore formation, a conductance state of ~14.3 nS was believed to be created by an aggregation of ~3.6 QDs and with a pore diameter ~6.09 nm (under a biasing voltage of -10 mV). Whereas, a lower conductance state (~6.3 nS) was also realized corresponding to an aggregation no.3 and with a spherical nanopore size of 4 nm. In contrast, in the model which is based on the creation of non-spherical pores, the respective conductance states were believed to be created by a relatively smaller diameter ~1.5 nm (QD aggregation of no. 2.6) and ~0.95 nm (aggregation no.2.4). By increasing the biasing voltage to -20 mV, the conductance values were increased to 11 nS and 21.1 nS which corresponded to 5.3 and 7.5 nm spherical pores, but of 1.22 nm and 1.8 nm as for diameters of the non-spherical pores. Thus, we predict that the non-spherical pores (d_{nspore}) can be a better approximation over spherical nanopores (d_{spore}) for exhibiting a definite conductance level. At times, even $d_{nspore} \leq 4d_{spore}$ and that the nonspherical nanopores were associated with a smaller no. of QDs than the case for spherical nanopores, for a definite conductance state. On the other hand, since an aggregation no. ≤ 3 is physically unrealistic in view of nanopore formation, the migration of ions could be stochastic due to non-static feature of the aggregated QDs owing to thermal effects.

-While the models, to a large extent, describe the QD induced nanopores and consequently, ion channel activity, more work in this direction is required to incorporate the effects due to QD size and shape distribution. *Once this is worked out, one can really get access to control the ion conducting pathways in a more precise way.* The voltage gated, ion channel activity generated by highly fluorescent CdSe QDs in naturally extracted lecithin-bilayer supported on a new substrate material would find ample scope in biochemical detection, DNA sequencing, cellular drug delivery and other electrophysiological applications.

References

1. Ludtke, S.J., et al., *Membrane pores induced by magainin*. Biochemistry, 1996. **35**(43): p. 13723-13728.
2. He, K., et al., *Mechanism of alamethicin insertion into lipid bilayers*. Biophysical journal, 1996. **71**(5): p. 2669-2679.
3. Bamberg, E. and P. Läuger, *Channel formation kinetics of gramicidin A in lipid bilayer membranes*. The Journal of membrane biology, 1973. **11**(1): p. 177-194.
4. Yeaman, M.R. and N.Y. Yount, *Mechanisms of antimicrobial peptide action and resistance*. Pharmacological reviews, 2003. **55**(1): p. 27-55.
5. Cantor, R.S., *Size distribution of barrel-stave aggregates of membrane peptides: influence of the bilayer lateral pressure profile*. Biophysical journal, 2002. **82**(5): p. 2520-2525.
6. Pouny, Y., et al., *Interaction of antimicrobial dermaseptin and its fluorescently labeled analogues with phospholipid membranes*. Biochemistry, 1992. **31**(49): p. 12416-12423.
7. Matsuzaki, K., et al., *An antimicrobial peptide, magainin 2, induced rapid flip-flop of phospholipids coupled with pore formation and peptide translocation*. Biochemistry, 1996. **35**(35): p. 11361-11368.
8. Boheim, G., W. Hanke, and G. Jung, *Alamethicin pore formation: voltage-dependent flip-flop of α-helix dipoles*. Biophysics of structure and mechanism, 1983. **9**(3): p. 181-191.
9. Laver, D.R., *The barrel-stave model as applied to alamethicin and its analogs reevaluated*. Biophysical journal, 1994. **66**(2, Part 1): p. 355-359.
10. Vodyanoy, I., J. Hall, and T. Balasubramanian, *Alamethicin-induced current-voltage curve asymmetry in lipid bilayers*. Biophysical journal, 1983. **42**(1): p. 71-82.
11. Fertig, N., et al., *Activity of single ion channel proteins detected with a planar microstructure*. Applied Physics Letters, 2002. **81**(25): p. 4865-4867.
12. Fertig, N., et al., *Microstructured apertures in planar glass substrates for ion channel research*. Receptors and Channels, 2003. **9**(1): p. 29-40.
13. Suzuki, H., et al., *Highly reproducible method of planar lipid bilayer reconstitution in polymethyl methacrylate microfluidic chip*. Langmuir, 2006. **22**(4): p. 1937-1942.
14. Fertig, N., R.H. Blick, and J.C. Behrends, *Whole Cell Patch Clamp Recording Performed on a Planar Glass Chip*. Biophysical journal, 2002. **82**(6): p. 3056-3062.
15. Mayer, M., et al., *Microfabricated teflon membranes for low-noise recordings of ion channels in planar lipid bilayers*. Biophysical journal, 2003. **85**(4): p. 2684-2695.
16. Uram, J.D., K. Ke, and M. Mayer, *Noise and bandwidth of current recordings from submicrometer pores and nanopores*. ACS nano, 2008. **2**(5): p. 857-872.
17. Qi, L. and X. Gao, *Emerging application of quantum dots for drug delivery and therapy*. Expert opinion on drug delivery, 2008. **5**(3): p. 263-267.
18. Alexson, D., et al., *Semiconductor nanostructures in biological applications*. Journal of Physics: Condensed Matter, 2005. **17**(26): p. R637-R656.
19. Jamieson, T., et al., *Biological applications of quantum dots*. Biomaterials, 2007. **28**(31): p. 4717-4732.
20. Li, Q., et al., *Tracking single quantum dot and its spectrum in free solution with controllable thermal diffusion suppression*. Analytical biochemistry, 2008. **377**(2): p. 176-181.
21. Klein, S.A., et al. *Formation of nanopores in suspended lipid bilayers using quantum dots*. in *Journal of Physics: Conference Series*. 2008: IOP Publishing.
22. Böckmann, R.A., et al., *Effect of sodium chloride on a lipid bilayer*. Biophysical journal, 2003. **85**(3): p. 1647-1655.
23. Ramachandran, S., et al., *Current bursts in lipid bilayers initiated by colloidal quantum dots*. Applied Physics Letters, 2005. **86**(8): p. 083901-083901-3.
24. Chen, F. and D. Gerion, *Fluorescent CdSe/ZnS nanocrystal-peptide conjugates for long-term, nontoxic imaging and nuclear targeting in living cells*. Nano letters, 2004. **4**(10): p. 1827-1832.
25. Poderys, V., et al., *Interaction of water-soluble CdTe quantum dots with bovine serum albumin*. Nanoscale Res Lett, 2011. **6**: p. 9.
26. Bihari, P., et al., *Optimized dispersion of nanoparticles for biological in vitro and in vivo studies*. Particle and Fibre Toxicology, 2008. **5**(1): p. 14.
27. Elgrabli, D., et al., *Effect of BSA on carbon nanotube dispersion for in vivo and in vitro studies*. Nanotoxicology, 2007. **1**(4): p. 266-278.
28. Shah, C.P., et al., *Precursor concentration and temperature controlled formation of polyvinyl alcohol-capped CdSe-quantum dots*. Beilstein journal of nanotechnology, 2010. **1**(1): p. 119-127.
29. Šimurda, M., et al., *Modification of carrier dynamics in CdSe nanocrystals by excess Cd in deposition bath*. Physica E: Low-dimensional Systems and Nanostructures, 2007. **36**(2): p. 205-210.
30. Gupta, P. and M. Ramrakhiani, *Influence of the particle size on the optical properties of CdSe nanoparticles*. Open Nanoscience Journal, 2009. **3**: p. 15-19.

31. Mansur, H.S., A.A. Mansur, and J. González, *Synthesis and characterization of CdS quantum dots with carboxylic-functionalized poly (vinyl alcohol) for bioconjugation.* Polymer, 2011. **52**(4): p. 1045-1054.

32. Feng, L., et al., *Petal effect: a superhydrophobic state with high adhesive force.* Langmuir, 2008. **24**(8): p. 4114-4119.

33. Sines, I.T., et al., *Colloidal Synthesis of Non-Equilibrium Wurtzite-Type MnSe.* Angewandte Chemie International Edition, 2010. **49**(27): p. 4638-4640.

34. Pradhan, N. and X. Peng, *Efficient and color-tunable Mn-doped ZnSe nanocrystal emitters: control of optical performance via greener synthetic chemistry.* Journal of the American Chemical Society, 2007. **129**(11): p. 3339-3347.

35. Furdyna, J.K., *Diluted magnetic semiconductors.* Journal of Applied Physics, 1988. **64**(4): p. R29-R64.

36. Heulings, H.I., et al., *Mn-substituted inorganic-organic hybrid materials based on ZnSe: Nanostructures that may lead to magnetic semiconductors with a strong quantum confinement effect.* Nano letters, 2001. **1**(10): p. 521-526.

37. Lei, S., K. Tang, and H. Zheng, *Solvothermal synthesis of α-MnSe uniform nanospheres and nanorods.* Materials Letters, 2006. **60**(13–14): p. 1625-1628.

38. Zhu, K., et al., *Manganese-doped MnSe/CdSe core/shell nanocrystals: Preparation, characterization, and study of growth mechanism.* Journal of Materials Research, 2011. **26**(18): p. 2400-2406.

39. Biswas, S., S. Kar, and S. Chaudhuri, *Optical and magnetic properties of manganese-incorporated zinc sulfide nanorods synthesized by a solvothermal process.* The Journal of Physical Chemistry B, 2005. **109**(37): p. 17526-17530.

40. Ji, Z., et al., *Dispersion and stability optimization of TiO2 nanoparticles in cell culture media.* Environmental science & technology, 2010. **44**(19): p. 7309-7314.

41. Petri-Fink, A., et al., *Effect of cell media on polymer coated superparamagnetic iron oxide nanoparticles (SPIONs): colloidal stability, cytotoxicity, and cellular uptake studies.* European journal of pharmaceutics and biopharmaceutics, 2008. **68**(1): p. 129-137.

42. Boonsongrit, Y., et al., *Controlled release of bovine serum albumin from hydroxyapatite microspheres for protein delivery system.* Materials Science and Engineering: B, 2008. **148**(1): p. 162-165.

43. O'Shaughnessy, T.J., et al., *Laser ablation of micropores for formation of artificial planar lipid bilayers.* Biomedical Microdevices, 2007. **9**(6): p. 863-868.

44. Wüthrich, R., et al., *Spark assisted chemical engraving (SACE) in microfactory.* Journal of Micromechanics and Microengineering, 2005. **15**(10): p. S276.

45. Suzuki, H. and S. Takeuchi, *Microtechnologies for membrane protein studies.* Analytical and Bioanalytical Chemistry, 2008. **391**(8): p. 2695-2702.

46. Patil, V.V., R.V. Galge, and B.N. Thorat, *Extraction and purification of phosphatidylcholine from soyabean lecithin.* Separation and Purification Technology, 2010. **75**(2): p. 138-144.

47. Ceci, L., D. Constenla, and G. Crapiste, *Oil recovery and lecithin production using water degumming sludge of crude soybean oils.* Journal of the science of food and agriculture, 2008. **88**(14): p. 2460-2466.

48. Montal, M. and P. Mueller, *Formation of bimolecular membranes from lipid monolayers and a study of their electrical properties.* Proceedings of the National Academy of Sciences, 1972. **69**(12): p. 3561-3566.

49. Robello, M. and A. Gliozzi, *Conductance transition induced by an electric field in lipid bilayers.* Biochimica et biophysica acta, 1989. **982**(1): p. 173-176.

50. Brzezinski, P., et al., *Charge displacements in interfacial layers containing reaction centers.* The Journal of membrane biology, 1998. **165**(3): p. 213-225.

51. Gramse, G., et al., *Nanoscale Measurement of the Dielectric Constant of Supported Lipid Bilayers in Aqueous Solutions with Electrostatic Force Microscopy.* Biophysical journal, 2013. **104**(6): p. 1257-1262.

52. Noronha, F.S., et al., *Macrophage damage by Leishmania amazonensis cytolysin: evidence of pore formation on cell membrane.* Infection and immunity, 2000. **68**(8): p. 4578-4584.

53. Chen, J., et al., *Cationic nanoparticles induce nanoscale disruption in living cell plasma membranes.* The Journal of Physical Chemistry B, 2009. **113**(32): p. 11179-11185.

54. Eaton, D.C., *Ionic channels of excitable membranes. Bertil Hille. Sunderland, Ma: Sinauer Associates, 1984.* Journal of Neuroscience Research, 1985. **13**(4): p. 599-600.

55. Kuyucak, S., O.S. Andersen, and S.-H. Chung, *Models of permeation in ion channels.* Reports on Progress in Physics, 2001. **64**(11): p. 1427.

56. Sarma, R. and D. Mohanta, *A Comprehensive View on the Brownian Motion of Quantum Dots in Electrolytic Solution, Lipid Bilayer and Their Aggregated State in the Lipid Biomembrane.* Journal of Computational and Theoretical Nanoscience, 2012. **9**(8): p. 1070-1077.

12. S&T benefits accrued:
    i.   List of Research publications

SL No	Authors	Title of paper	Name of the Journal	Volume	Pages	Year
1.	Runjun Sarma and Dambarudhar Mohanta	A Comprehensive View on the Brownian Motion of Quantum Dots in Electrolytic Solution, Lipid Bilayer and Their Aggregated State in the Lipid Biomembrane	*Journal of Computational and Theoretical Nanoscience* DOI: *10.1166/jctn.2012.2145*	9 (8)	1070-1077	2012
2.	Runjun Sarma and Dambarudhar Mohanta	Role of the Supporting Substrates for Implementing Planar Chip Technology in Ion Channel Experiments	*International Journal of Advanced Materials Science*	3 (2)	87-96	2012.
3.	R. Sarma, A. Chetry, and D. Mohanta,	Synthesis, stabilization of CdSe quantum dots and role of rose water and citric environment	*Nanoscience and Nanotechnology Letters* DOI: *10.1166/nnl.2012.1397*	3(8)	775-782	2012
4.	Runjun Sarma and Dambarudhar Mohanta	Recording ion channels across soy-extracted lecithin bilayer generated by water-soluble quantum dots	*Philosophical Magazine* DOI: *10.1080/14786435. 2013.853140*	94	345-357	2014
5.	R. Sarma, Q. Das, A. Hussain, A. Ramteke, A. Choudhury, D. Mohanta	Physical and Biophysical Relevance of Water Soluble, Highly Fluorescent Manganese Selenide Quantum Dots	*Nanotechnology* DOI: *10.1088/0957-4484/ 25/27/275101*	25	275101 and 359601	2014

Conference Attended

1. "A comprehensive study of Brownian motion of quantum dots in electrolytic solution, lipid bilayer and their aggregated state in lipid biomembrane" NCSN, 2011, Tezpur University, Assam.

2. " Interaction of CdSe quantum dots with soy-extracted lecithin" National Symposium on Nanobiotechnology, 2012, IIT Mandi, Himachal Pradesh.

3. "Role of substrate supports for implementing planar chip technology in ion channel experiments", CMDAYS, 2010, Kalyani University, Kolkata.

ii.   Manpower trained on the project
     a) Research Scientists or Research Associates
     b) No. of Ph.D. produced: (01) Thesis in preparation by Ms R. Sarma
     c) Other Technical Personnel trained

iii.   Patents taken, if any

13. Financial Position:

No	Financial Position/ Budget Head	Funds Sanctioned (Rs)	Expenditure (Rs)	% of Total cost
I	Salaries/ Manpower costs	4,56,000/-	4,56,000/-	
II	Equipment	11,00000/-	**12,47,255/-	
III	Supplies & Materials/consumables	60,000/-	40,732/-	100%
IV	Contingencies	45,000/-	44,979/-	
V	Travel	39,000/-	27,496/-	
VI	Overhead Expenses	3,40,000/-	1,93,538/-	
VII	Others, if any			
	Total	*20,40,000/-	20,10,000/-	

* Actual amount received: 20, 10,000/-

** Excess expenditure is Rs.1,47,255/- against Equipment Head was adjusted against Overhead Expenses

14. Procurement/ Usage of Equipment (a)

S No	Name of Equipment	Make/Model	Cost (FE/ Rs)	Date of Installation	Utilisation Rate (%)	Remarks regarding maintenance/ breakdown
1.	Minor equipment, EPC 10 Patch Clamp Amplifier, Patchmaster software FITMASTER etc.	Make: HEKA Elektronik, Dr Schulze GmbH, Wiesenstraße 71	12,47,255/-	23/6/2011	60 %	NA

b) Plans for utilizing the equipment facilities in future

-To Study the QDs ion channel formed by nonspherical QDs

-To study ion channels under external field (static magnetic field, light etc.)

13.11.13

Name and Signature with Date
(Principal Investigator)